Analytic and raytrace modeling of a miniaturized infrared spectrometer module

Kimmo Keränen*, Martti Blomberg**, Jussi Tenhunen* and Pentti Karioja***

*VTT Electronics, 90570 Oulu, Finland, kimmo.keranen@vtt.fi, jussi.tenhunen@vtt.fi
** VTT Electronics, FIN-02044 VTT, Finland, martti.blomberg@vtt.fi
*** VTT Electronics&Infotech Oulu, 90570 Oulu, Finland, pentti.karioja@vtt.fi

ABSTRACT

When designing the construction of an optoelectronic module, the modeling of the system allows for the possibility to optimize geometries, materials and components in order to achieve optimal performance and cost effectiveness for the final product. We use an approach in which an analytical model and simulation model supplement each other in order to speed up and enchance the device development process. Our system integrator approach consists of analytical modeling and raytrace simulation modeling of the system, system realization and system characterization.

Our pilot miniaturized system comprised three silicon micromachined devices: an electrically modulated thermal infrared emitter, an electrically tunable Fabry-Perot interferometer (FPI) and a photodetector.

Analytic modeling of the system was verified by optical simulation software raytracing. The simulation results were verified by experiments thus enhancing the development of the simulation model.

Keywords: Modeling, optimization, miniaturization, spectrometer, module.

1 INTRODUCTION

The main reasons for the miniaturization of optoelectronic systems are the following [1]

- customer needs determine that the size and weight of the systems has to be reduced,
- the optimization of system performance and price are best achieved by device miniaturization,
- the miniaturization gives system potential for new applications.

System optimization by iterative design process associated with simulations enhances the cost effectiveness of the miniature system development. In our pilot case, the optimization of performance means that the spectrometer parameters are optimized for specific application. In practice, this means that the transmission of the spectrometer system, the emittance of the source and the response of the detector are optimized for the specific reference and absorption wavelength bands.

The cost of a final system is depending on the size of the manufacturing lot and the manufacturing technology [2]. The use of silicon micromachined devices is advantageous in large volume applications. Integration of devices to same chip decreases system size, increases reliability and further reduces the system cost.

System flexibility and enhanced system application potential can be achieved through the combination of micro optics and micro mechanics with electronics, which paves the way for a new class of micro-electro-mechanical devices [3] and innovative sensors [4],[5].

2 BASIC DEVICES OF THE SPECTROMETER

The miniaturized multipurpose spectrometer, (Fig. 1), comprises three silicon micromachined devices: the electrically modulated thermal infrared emitter, the electrically tunable Fabry-Perot interferometer (FPI) and the photodetector. In addition, an IC circuit is die-bonded and wire-bonded on a silicon substrate.

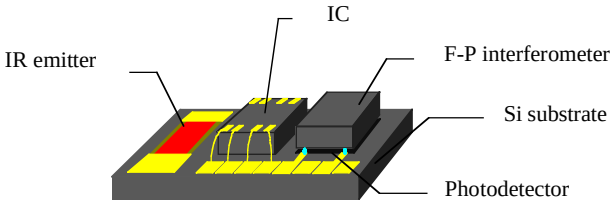

Figure 1. The miniaturized spectrometer.

The size of the infrared emitter is 1 mm x 1 mm. The emitter consists of several emitting wires with 1-µm thickness, 20-µm width and 1000-µm length. The infrared emitter was monolithically integrated into the silicon substrate. The operating temperature of the emitter was about 973 K.

The silicon micromachined FPI device is an optical resonator consisting of two parallel mirrors separated by a Fabry-Perot cavity. The transmission band of the device is controlled by changing the separation of the mirrors. The separation of the mirrors can be changed by electrostatic force by applying a voltage between the mirrors. The structure of the FPI device is shown in Fig. 2. The size of the FPI chip was 3.3 mm x 3.3 mm x 0.5 mm. The active area diameter was 0.75 mm. The typical transmission of the FPI was 65% and the typical FWHM band pass was 70 nm, when Numerical Aperture (NA) 0.2 was used. A 20% tuning range of the nominal wavelength, 95% transmission

and a 25 dB contrast can be obtained. A more detailed description of the FPI device is presented in Ref. 6.

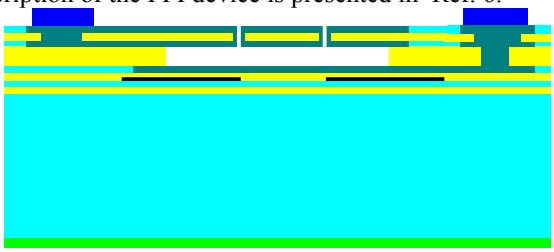

Figure 2. The cross-section of the surface micromachined FPI device.

The infrared detector was a bolometer monolithically integrated into the silicon substrate. The size of the bolometer was 1.5 mm x 1.5 mm, and the diameter of light sensitive area was 0.6 mm. The temperature sensitive resistor was in the middle of the light sensitive area, and its measures were 25 µm x 90 µm. The response of the detector was 3…5 V/W with a calibrated 1000 K blackbody source.

The integrated circuit was a commercial operational amplifier manufactured by Analog Devices, type AD797. The function of the IC is to act as pre-amplifier of the detected signal.

3 SYSTEM MODELING

System optical modeling was performed in two steps. Firstly, an analytical model of the system was created using Mathcad software. The infrared source was assumed as blackbody radiator in this model. Secondly, a raytrace model was created using ASAP PRO 6.0 optical design and simulation software. The purpose of the optical modeling was to determine the critical optical characteristics of the system in order to optimize the system performance. The following issues were tested in the optical simulations

1. optical power efficiency from source to detector (through the FPI device),
2. optical crosstalk from source to detector (excluding the FPI device),
3. incident light angular distribution on the FPI surface.

3.1 Analytical model of the system

In order to estimate the optical power efficiency from source to detector an analytical model of the system was derived treating the thermal infrared emitter as greybody radiator [6]. Greybody emitter's spectral shape matches that of a true blackbody, but its absorptance is less than 1.0.

The emitter's absolute temperature was 973 K. The total radiant flux emitted from the surface of an object at this temperature can be expressed by the Stefan-Boltzmann law, in the form

$$M_{bb} = \sigma T^4, \tag{1}$$

where M_{bb} is the exitance of the emitter surface in a vacuum, σ is the Stefan-Boltzmann constant, and T is the temperature in degrees kelvin A blackbody at 973 K emits at the rate of 50823 W/m^2.

Planck's blackbody spectral radiation law accurately predicts the spectral radiance of blackbodies in a vacuum at any temperature in the form

$$L_{bb\lambda} = \frac{\varepsilon 2hc^2}{\lambda^5 (e^{\frac{hc}{\lambda kT}} - 1)}, \tag{2}$$

where ε is the emittance coefficient of the source, h is the Planck's constant, c is the speed of light in a vacuum, and k is Boltzmann's constant.

Inserting the values of constants into the equation 2 and multiplying by π and giving the wavelength in µm, we get spectral exitance of the emitter

$$M_{bb\lambda} = \frac{3.741 \leftarrow 10^8}{\lambda^5 (e^{14388/\lambda T} - 1)}. \tag{3}$$

If the specific wavelength is 4.5 µm, the spectral exitance of the emitter is 7877 W×m^{-2}×µm^{-1}. Assuming circular emitter area, the size of which is the same as the detector, we get 0.16 mW at 70 nm wavelength band. Assuming ideal optics without any aberrations and transmission losses, it is possible to transfer part of this power through the FPI to the surface of the detector. Ideal optics means that the power inside the solid angle of the collecting optics is transmitted totally through the optical system. If the FPI NA of 0.2 is not exceeded by the imaging optics, the optics F-number is limited to 2.5 in 1:1 imaging. Approximating the infrared emitter as a point source about 2% of the infrared emitter's total radiant power is possible to collect and transmit to the detector by the optics. If the FPI transmittance is 65%, the detector response 5 V/W and the voltage amplification 570, then the signal value will be 5.9 mV.

The analytical model to the optical crosstalk of the system was not possible to generate and optical crosstalk was examined only by the raytrace model.

In order to estimate the effect of the incident light angular distribution on the surface of the FPI an analytical model of the FPI transmittance as a function of angular distribution was created. FPI transmission spectrum for a plane wave is following [7]

$$T_{FPI}(\lambda, d, \theta, R, A, n) = \left(1 - \frac{A}{(1-R)}\right)^2 \frac{(-1+R)^2}{(-1+R)^2 + 4R\left(\sin\left(2\pi n d \frac{\cos(\theta)}{\lambda}\right)\right)^2} \tag{4}$$

Average transmission in a converging beam is following

$$T_{FPI\theta}(\lambda, d, \theta_{max}, R, A, n) = \frac{\int_0^{\theta_{max}} T_{FPI}(\lambda, d, \theta, R, A, n) 2\pi\theta d\theta}{\int_0^{\theta_{max}} 2\pi\theta d\theta}. \tag{5}$$

Simulated average transmission of the FPI, when converging beam half angle θmax is 0.1°, 5.7°, 11.5° and 17.5°, is shown in Fig. 3.

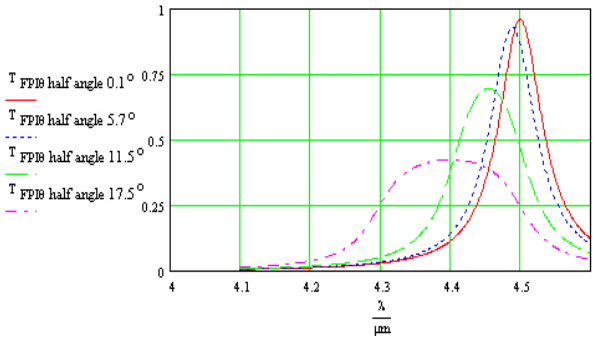

Figure 3. Average transmittance of the FPI, when the beam half angle θmax is 0.1°, 5.7°, 11.5° and 17.5°.

As one can see from Fig. 3 the transmission peak lowers, transmission peak spreads and moves towards shorter wavelengths, when the converging beam half angle increases. A maximum value of 11.5 degrees for the converging beam half angle is suggested.

3.2 Raytrace model of the system

The raytrace system model was build in the ASAP PRO 6.0 environment.

According to simulations, the optical power efficiency from source to detector was 0.4% without the cover. Approximation with a point source with an ideal optics gave the efficiency of 2%. The difference is mainly caused by the spherical aberration of the mirror and the fact that the transmission losses were ignored in the analytical modeling.

According to the simulations carried out to the system shown in Fig. 4, the normalized optical crosstalk level obtained was 1:12000 at maximum. This is a reasonably good value for system realization. One reason for such a low optical crosstalk value was that a gap was realized to the substrate near the emitter. This gap blocks most of the rays which are propagating from emitter to the detector through the silicon substrate.

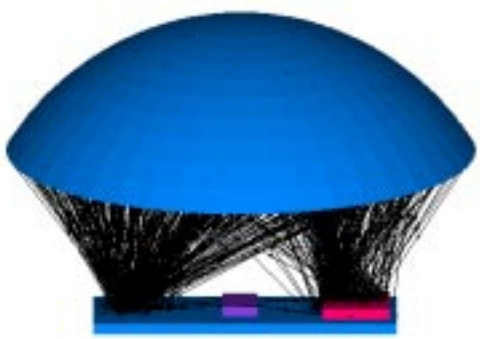

Figure 4. The 3D-raytrace model of the system with spherical mirror.

The angular distribution of rays entering the clear aperture of the FPI is shown in Fig.5.

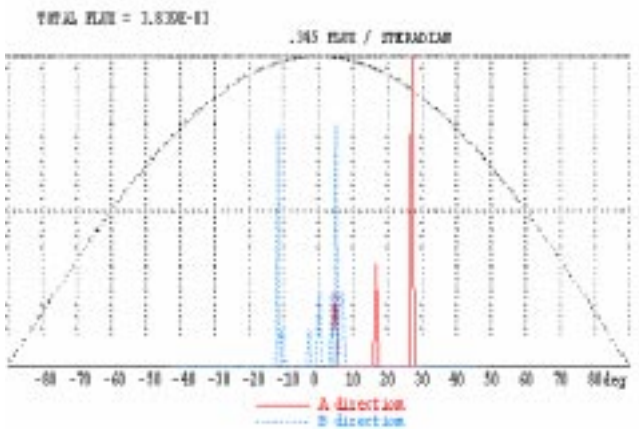

Figure 5. Optical power level and angular distribution of the incident rays at the surface of the detector.

In the Fig. 5 we can see the angular distribution of the incident rays in two directions, A and B, at the detector surface. A Lambertian source flux is seen as a reference. We can see from Fig. 5 that some part of the incident light has actually too large an angle of incidence compared to maximum suitable NA of the FPI. In order to optimize angle distribution, a 2 mm aperture at a distance of 5 mm from FPI, was needed. This kind of aperture could be integrated into the cover of the spectrometer module.

4 SYSTEM REALIZATION

The packaging schematics of the spectrometer module is shown in Fig. 6.

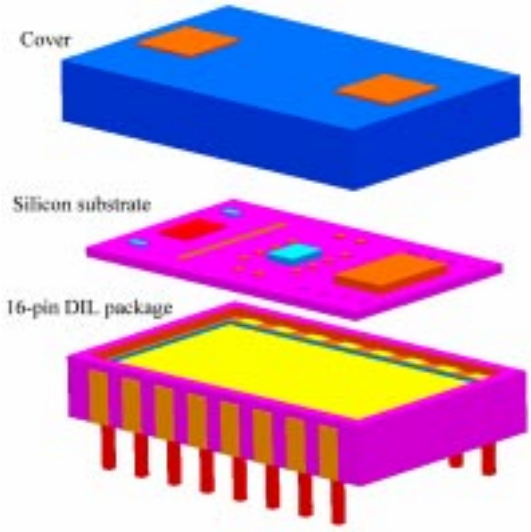

Figure 6. The packaging schematics of the spectrometer module.

The silicon substrate, in which the thermal emitter and detector were integrated and on which the FPI device was flip-chip bonded and the IC chip was die-bonded, was mounted in a 16-pin DIL package. The DIL package was

manufactured by Kyocera, model KD-75336-D, and it was covered with a lid having separate silicon windows for the source and the detector.

5 CHARACTERIZATION OF THE SPECTROMETER

In the measurements, the spectrometer IC was used as a pre-amplifier of the system. Biasing electronics, operating voltage electronics and filtering electronics were placed on a FR4 based board, which also contained a base for the 16-pin DIL spectrometer module. The IR-emitter was driven by 50/50 square pulses at a frequency from 0.1.Hz to 20 Hz. A mirror was placed above the spectrometer to couple the light from the source to the detector through the dispersive FPI device. The detected signal was amplified by the pre-amplifier and the signal was amplified further by a post-amplifier and detected by a phase-locked amplifier, Stanford Research System's model SR830.

Total electrical amplification in the system was 570. When modulating the source at 5 Hz, the detected optical signal level at a reference band was 1 mV and peak-to-peak noise level was 10 μV resulting in a 100 signal-to-noise ratio at 1 Hz bandwidth. The simulated transmission value of the system was 0.4%, which would give 1.2 mV signal as a result. Thus, the measured signal value was 83% of the raytrace simulated one, which is in good agreement with the simulation.

In the measurements, the detected signal had about a 3 mV offset level when the source was modulated at the 0.1...20 Hz frequency band. This was due to the fact that the electrical driving pulses of the emitter were directly detected by the biased detector and further amplified by the system. Thus, the offset signal arises from the electrical crosstalk of the system. Crosstalk coupling from the emitter drive circuitry to the detector electronics seemed to be capacitive coupling via the silicon substrate. The effect of electrical crosstalk, however, was attenuated when sinusoidal driving was used in the emitter driving. The use of sinusoidal driving reduced the electrical crosstalk level by about 30 dB from the value obtained when using square wave driving.

6 DISCUSSION

The integration of an optical emitter into the same substrate with a detector is a good move from the miniaturization and modularization point of view, but it might introduce signal coupling through the substrate from the source to the detector as happened in our system. This kind of electrical crosstalk effect is also possible to detect and optimize by means of modern simulation tools. Our opinion is that in order to realize the micro-opto-electro-mechanical system (MOEMS) succesfully, the system design has to be simulated properly by mechanical. optical and electrical simulation tools in order to achieve optimized design by the iterative design process.

7 CONCLUSIONS

The analytical model of the system power budget forms a base for the raytrace model power budget. Optical throughput estimation of the system was possible to attain by the analytical model but the raytrace model gave roughly five times better estimation of the actual throughput than the analytical model. A good agreement between the ray trace model and the experimental signal level was obtained.

The optical crosstalk estimation of the system wasn't possible to produce by the analytical model and therefore it was produced only by the raytrace model. The raytrace model proved that the optical crosstalk level is insignificant in the system.

The analytical model of the average transmission of the FPI was created. This model showed that system performance is strongly depending of the actual NA of the FPI. Therefore actual NA of the FPI was examined by the raytrace model. The raytrace model indicated that suitable NA of the FPI was exceeded. Therefore a optimized cover structure was suggested in order to optimize angle distribution at FPI.

REFERENCES

[1] H. Kopola, P. Karioja, O. Rusanen, A. Lehto and J. Lammasniemi, "Hybridization, assembling, and testing of miniaturized optoelectronic modules for sensors and microsystems," in: Motamedi, M.E. & Goering, R. (eds.), Miniaturized Systems with Micro-Optics and Micromechanics III. Proc. SPIE Press, Bellingham, Vol. 3276, 56–64, 1997.

[2] S.H. Lee and W. Daschner, "Low cost high quality fabrication methods and CAD for diffractive optics and computer holograms compatible micro-electronics and micro-mechanics fabrication", in S. Martellucci and A. N. Chester (eds.) Diffractive Optics and Optical Microsystems, Plenum Press, New York, 133-138, 1997.

[3] M. E. Motamedi, "Merging micro-optics with micromechanics: micro-opto-electro-mechanical (MOEM) devices", in S.H. Lee (ed.), Diffractive and Miniaturized Optics, Proc. SPIE Press, Bellingham, Vol. CR49, 302-328, 1994.

[4] K. Keränen, P. Karioja, O. Rusanen, J. Tenhunen, M. Blomberg and A. Lehto, "Electrically Tuneable NIR-spectrometer" in: Parriaux, O.M., Kley, E-B., Culshaw, B., Breidne, M. (eds.) Micro-optical Technologies for Measurement, Sensors, and Microsystems II., Proc. SPIE. Press, Bellingham, Vol. 3099, 181-184, 1997.

[5] M. Blomberg, M. Orpana and A. Lehto, "Electrically tunable Fabry-Perot interferometer produced by surface micromechanical techniques for use in optical material analysis", US Patent # 5,561,523, 1996.

[6] R. McCluney, "Introduction to Radiometry and Photometry", Artech House, Norwood, 63-66, 1994.

[7] E. Hecht, "Optics", Addison-Wesley Publishing Company, Reading, 368-371, 1990.